



## Contribution of deformation-induced martensite to fracture appearance of austenitic stainless steel

A. Das

To cite this article: A. Das (2016) Contribution of deformation-induced martensite to fracture appearance of austenitic stainless steel, *Materials Science and Technology*, 32:13, 1366-1373, DOI: [10.1080/02670836.2015.1126048](https://doi.org/10.1080/02670836.2015.1126048)

To link to this article: <http://dx.doi.org/10.1080/02670836.2015.1126048>



Published online: 03 Feb 2016.



Submit your article to this journal [↗](#)



Article views: 107



View related articles [↗](#)



View Crossmark data [↗](#)



Citing articles: 1 View citing articles [↗](#)

# Contribution of deformation-induced martensite to fracture appearance of austenitic stainless steel

A. Das\*

Fracture surface commonly carries the evidence of high-energy (ductile/tough) and low-energy (brittle) regions involved in fracture history, the macroscopic appearance of a fracture surface has often been utilised to qualitatively evaluate *toughness* of materials. For metastable austenitic stainless steels (AISI 304LN), the degree of martensitic transformation affects the fracture appearance and thus depends critically on the strain rate. The two dimensional *ductile tearing ridge* pattern quantified from many tensile fractographs are observed to predict the nature of disparity in deformation and fracture responses with systematic variation in strain rate of the steel under ambient atmosphere. The spatial distribution of deformation-induced martensite under tension at various stress/strains and strain rates strongly influences void nucleation, growth, coalescence and hence, keeps the *impression* on the *ductile tearing ridge* morphologies and dimple geometries on the fracture surface, where the initial inclusion content was constant.

**Keywords:** Ductile fracture, Strain rate, Deformation induced martensite, Dimple, Ridge pattern

## Introduction

The fracture energy is rationally a good indicator of the *structural integrity* assessment. The loading rate, loading mode, temperature and environment usually influence the fracture appearance of an alloy under service. Fracture, the *culmination* of any continued deformation route, is the division of any object into two or more pieces under externally applied load. Therefore, the fracture surface should hold the *signature* of the entire deformation history that was imposed to the object. The initiation of micro void is strongly dependent upon the existence of heterogeneities of defects (i.e., initial void volume fraction, second phase particles, phase interfaces, dislocation pile ups, grain boundary triple junctions, twin boundaries, shear band intersections, etc.) originally present in the alloy or their successive evolution during plastic deformation. In metastable austenitic stainless steels, formation of deformation-induced martensites (DIM) is reported to play an important role in damage accumulation and contributes to the style in which further deformation will take place and ultimately fracture.<sup>1-3</sup>

This communication precisely explores the correlation between the measured ductile fracture ridge area on the

fracture surfaces, the extent of deformation-induced phase transformation and the mechanical properties in austenitic stainless steel under tension at various strain rates under ambient temperature to establish the close association between deformation, solid state phase transformation and fracture.

In ductile fracture route, a mode of failure normally occurs through continual damage accumulation involving three distinct stages: void nucleation, growth and coalescence to shape a continuous fracture path/ridge.<sup>4-14</sup> The central philosophy of the inter-relationship between the deformation properties and the fracture process of different alloys under diverse conditions has been well documented by the present author elsewhere.<sup>1-3,9-14</sup> For ductile fracture, the engineering properties are principally determined by the interaction of stress and strain fields with the correspondingly developed microstructural features of the material. The connectivity between dimple size distribution/number densities and precipitate size/shape distribution has been established for a number of alloys reported by Goods and Brown in their elegant study.<sup>6</sup> Garrison *et al.*<sup>5,8,15-17</sup> experimented and reviewed the ductile fracture mechanisms of various alloys with fine scale microstructure and different void nucleation characteristics of steels/other alloys in their research works. The present author has already confirmed the correlation between mechanical properties and the micro void features of a ductile fracture for different alloys under unlike circumstances documented elsewhere.<sup>1-3,12-14</sup>

The fracture surfaces of materials failing by ductile manner are essentially covered by the segments of dimples

Fatigue & Fracture Group, Materials Science & Technology Division, CSIR-National Metallurgical Laboratory, Jamshedpur 831 007, Jharkhand, India

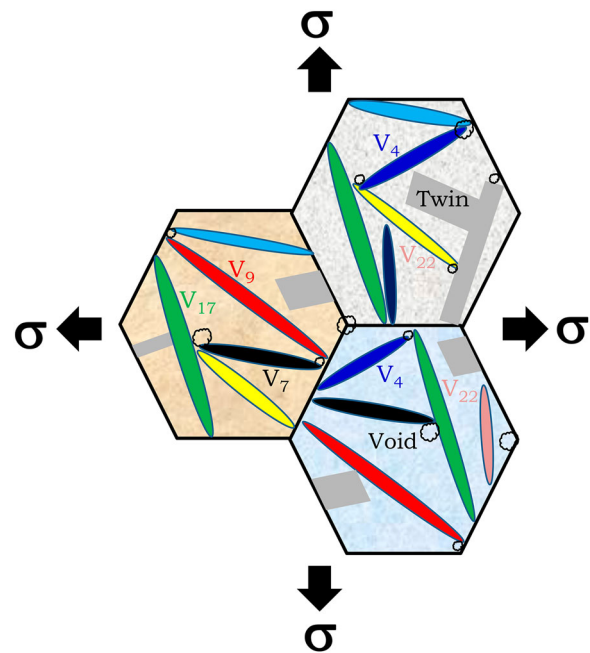
Current address: Mechanical Metallurgy Division, Materials Group, Bhabha Atomic Research Centre (Department of Atomic Energy), Trombay, Mumbai 400 085, Maharashtra, India.

\*Corresponding author, emails [dasarpan1@yahoo.co.in](mailto:dasarpan1@yahoo.co.in); [arpand@barc.gov.in](mailto:arpand@barc.gov.in)

which coalescence to produce the fracture path consisting of *ductile tearing ridge* network connected in three dimensions. The different sized dimples are normally separated by these tearing ridge patterns. These tearing ridges generally signify the boundaries of dimples spread throughout in three dimensions where different planes on the fracture have been intersected. The tearing ridges on the fracture surface are usually used to locate the crack initiation sites and its propagating path. Ideally, these tearing ridges testify to the inhomogeneous stress-state/strain-state distribution on the fracture surfaces. Present author has already reported the correlation between the two dimensional wear damage accumulations (i.e., impressions of ploughing lines/ridges along with debris fraction on worn surfaces) with the corresponding wear properties at various loading conditions for different grades of magnesium alloys.<sup>18</sup>

Cottrell<sup>19</sup> reported in his elegant study that the ligaments between growing voids would simply neck down to a *point*. Thus, a fracture surface of such failure would be dimples of a rather uniform size and spacing with the *ductile tearing ridges* pattern around the dimples representing the material drawn to a knife-edge fracture of zero cross-sections. Usually, the apparent *signature* of the shear localisation and the shear fracture is a fracture surface consisting of fine, closely spaced, submicron sized dimples whose widths are much larger than their depths. Slow fracture is generally rougher and is more likely to show greater evidence of *ductile tearing ridges*. Hence, it is logical to correlate the extent of *ductile tearing ridge* morphologies on the fracture surfaces in two dimensions with the corresponding mechanical and fracture properties of the material with the loading speed.

Voids initiate and grow at inclusions, precipitates and other second-phase particulate matter under the influence of plastic strains and hydrostatic tensile stress, which is well established. The distribution, size, shape, orientations and coherency of critical constituents present and/or generated during plastic deformation in the microstructure play an important role in the process leading to eventual fracture of a ductile material.<sup>6</sup> The localised *stress-state* and *strain-state* conditions required for nucleating voids strongly depend on the size, shape, orientation, location, internal fracture toughness and the interfacial strength of the inclusion or the second-phase particles present in the material. Schematic representation of void nucleation in deformed stainless steels under tension is shown in Fig. 1. It has been found that voids are nucleated at phase interfaces, grain boundary triple junctions, twin interfaces, etc. According to Garrison and Moody,<sup>5</sup> even if the material contains only one type of second-phase particle, void nucleation will not occur simultaneously at all of the particles. Benzerga *et al.*<sup>20</sup> explained that the fracture is strongly influenced by void shape, void spacing, stress triaxiality and strain hardening. It has also been investigated by the present author that void can even nucleate from grain boundaries or grain boundary triple junctions under creep deformation of primary reformer tube materials.<sup>21</sup> Typically, voids nucleate at the larger particles first. Voids nucleated at larger particles grow while voids are nucleated at the smaller particles as the fracture progresses under tensile stress.<sup>5</sup> The void growth stage involving relatively homogeneous plastic deformation of the matrix surrounding the voids is interrupted by the localisation of the plastic flow in the ligament



1 Schematic representation of different void nucleation sites adjacent to the martensite-austenite interfaces, grain boundary junctions, twin boundary, etc. Variants (martensite) numbers are arbitrary. All grains are not of equal sized

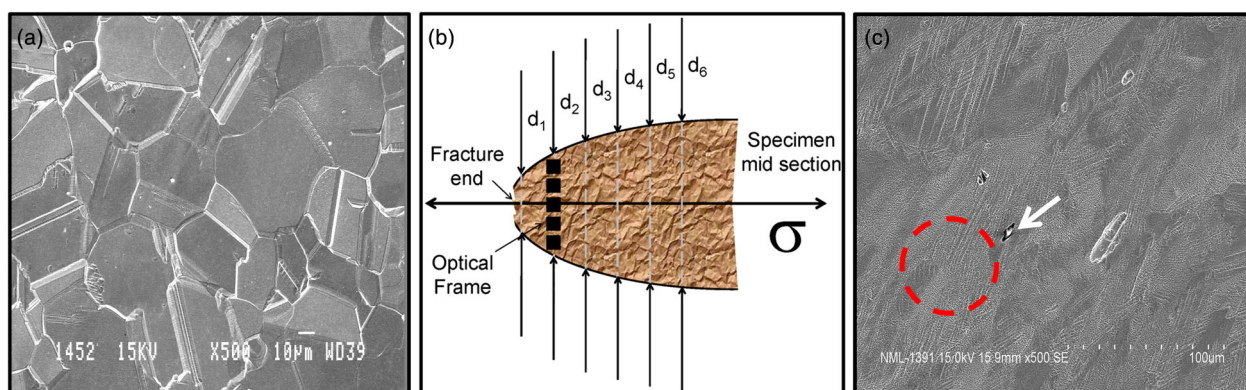
between the voids, which is nothing but the *ductile tearing ridge* features.<sup>22</sup> Cottrell<sup>19</sup> has pointed out that the plastic voids/cavities should be considered as numerous internal necks which grow, by plastic deformation, to meet the neighbouring voids and thus form a fracture surface without any real break or fracture taking place. Deformation paths at various strain rates would also play an important role in controlling not only the mechanical behaviour of the material, but also the void nucleation and growth mechanisms. According to Curry *et al.*,<sup>23</sup> the loading rate can have a significant influence on the fracture behaviour of ferritic steels at ambient temperature. The loading rate clearly determines the dislocation activities, configurations, etc., during and after deformation and hence, the variation in the microstructures.

In order to test the hypothesis that the ductile fracture features can be related to the mechanical and fracture properties of the material, it is necessary to systematically vary the density and type of void-initiating particles contained or generated during deformation in a microstructure. Such a fundamental scheme has been implemented in metastable AISI 304LN austenitic stainless steel through tensile tests at various strain rates under ambient temperature to systematically vary the size, shape, orientation, aspect ratio, amount and the distribution of DIM plates in an austenite matrix, which directly contributes to void nucleation where the initial inclusion content was constant for all the samples. In this study, the fracture features were considered to be the dimple geometry and the extent of *ductile tearing ridge* morphology in two dimensions. This research clearly indicates the novelty to the point where the mechanical and fracture properties of a material can be obtained from the two dimensional fracture feature analysis with reasonable accuracy. This study can be enormously helpful for the failure analyst.

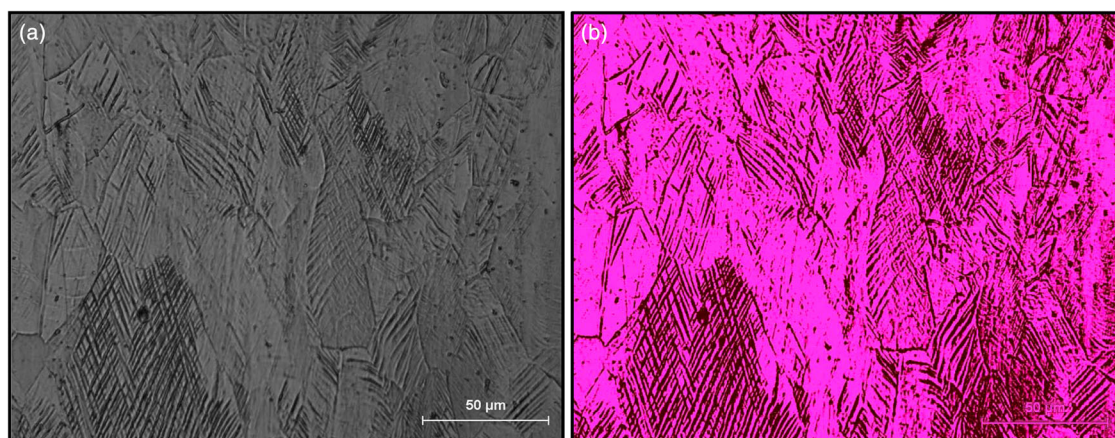
## Experimental

Nuclear grade AISI 304LN metastable austenitic stainless steel has been evaluated for the present research. The chemical composition (in wt.%) of the alloy is: C 0.03, Mn 1.78, Si 0.65, S 0.02, P 0.034, Ni 8.17, Cr 18.73, Mo 0.26, Cu 0.29, N 0.08 and the balance Fe. Initial austenite grain size (intercept length) of the material was measured as approximately 70  $\mu\text{m}$ . This material generally consists of polycrystalline austenite grains with a large number of annealing twins (shown in Fig. 2a). The mechanical properties of AISI 304LN stainless steel at various strain rates have been measured through tensile experiments at ambient and high temperatures, which have been reported by the present author elsewhere.<sup>1–3</sup> Fracture surfaces were analysed through secondary imaging in scanning electron microscope (SEM) for all the samples. Detailed discussions are made available elsewhere.<sup>1–3,12–14</sup> From the broken pieces, several thin slices (i.e., chopped like salad, approximately 1–2 mm width) were extracted from the fracture end up to the uniformly deformed region for all the fractured specimens at different strain rates.<sup>3</sup> All the thin slices were polished carefully and slowly in emery paper to remove the surface

roughness and cleaned with acetone in ultrasonic bath for several times. All the thin slices were handled carefully so that there will not be any contaminants sticking on it. Void density fraction has been measured for all the slices repetitively through Archimedes's principle. The details have been discussed elsewhere.<sup>3</sup> True plastic strain for all the slices have been measured by the equation:  $\epsilon = 2\text{LN}(D_0/D)$ ,<sup>24</sup> where  $D_0$  is the original diameter and  $D$  is the slice diameter. Other halves of fractured tensile specimens were longitudinally sectioned along the approximate mid-plane, polished and etched with a mixture of HCl and HNO<sub>3</sub> in 2:1 ratio. The schematic illustration of specimen mount is shown in Fig. 2b. A few drops of ethanol was used to reveal the DIM under SEM microscope, shown in Fig. 2c. Figure 2a was obtained by etching with HCl:HNO<sub>3</sub> = 2:1 solution. Extensive image processing has been performed on the etched optical micrographs obtained from the cross-sectional planes along the specimen axis and parallel to the fracture surface for quantitative information on DIM in specimens tested at different strain rates, which has been shown in Fig. 3. The details have been reported elsewhere.<sup>1–3</sup> Figure 3a shows a typical optical microstructure of deformed austenite consisting of two different phases:



2 a SEM (secondary image) microstructure of AISI 304LN austenitic stainless steel showing metastable polygonal austenitic grains and annealing twins, b schematic of metallographic sample inside the mount for quantifying DIM volume fraction at various stress/strain levels and c SEM microstructure of deformed AISI 304LN austenitic stainless steel showing DIM morphologies (red encircled) and void nucleation sites (arrow)



3 a Optical microstructure of AISI 304LN austenitic stainless steel after deformation (at strain rate of 0.001 s<sup>-1</sup>) showing DIM plates (black) under austenite matrix (grey) and b image processed micrograph for quantification of volume fraction of DIM plates (brown) in austenite matrix (pink)

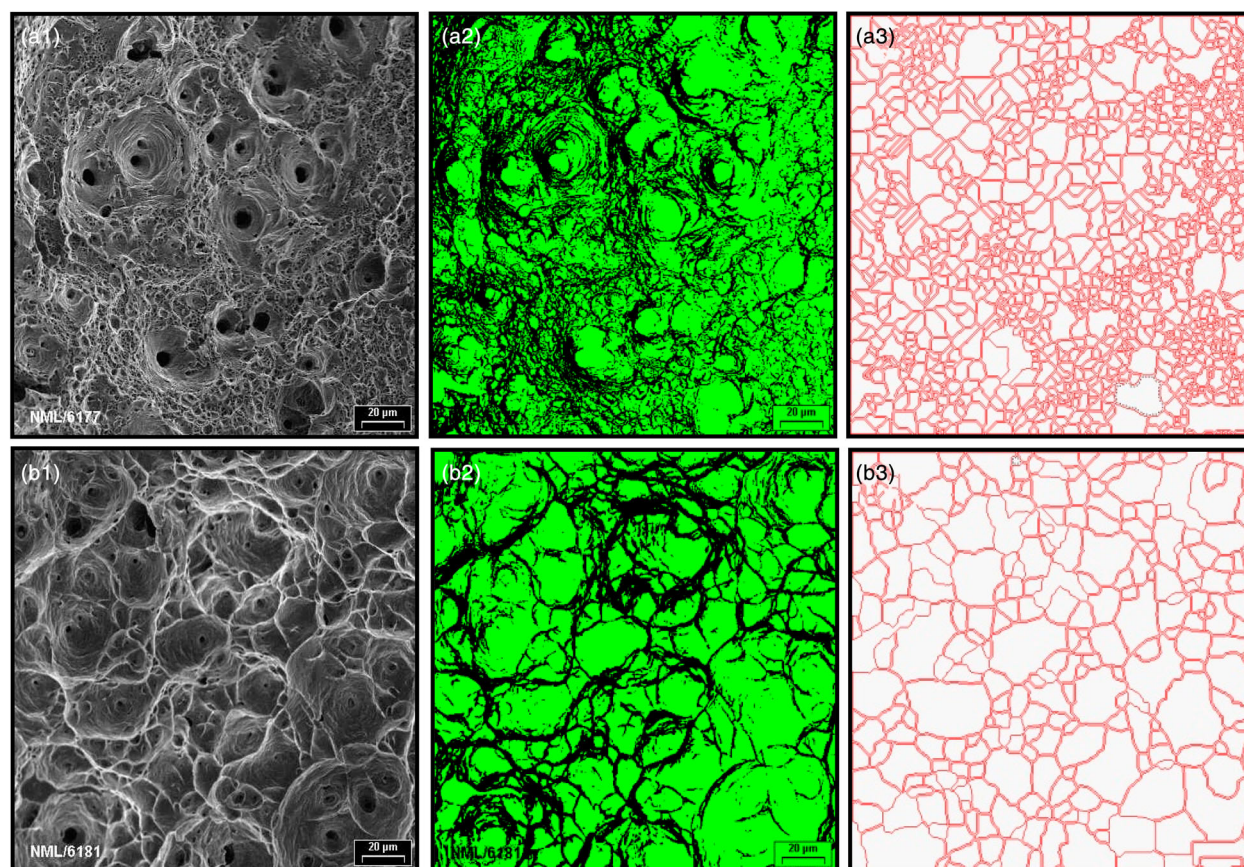
austenite (grey) and martensite (black). Figure 3b represents the image processed micrographs clearly distinguishing the martensite laths (brown) and polygonal austenite (pink) phases. The detailed discussions are available elsewhere.<sup>1-3</sup>

Typical metrics of coalesced dimples (Fig. 4a1 and b1) and the extent of ductile tearing ridge morphologies in two dimensions (Fig. 4a2 and b2) on the tensile fracture surfaces have been obtained through extensive image processing and linear intercept/point count methods on representative fractographs for all strain rates. In Fig. 4, only for two different strain rates' specimens are shown. The extent of ductile tearing ridge (Fig. 4a2 and b2) is simply a relative measurement of fracture features. With the advancement in the image processing technique, this information on the fracture surface can be re-claimed and used to understand the mechanical behaviour of material and this forms the purpose of this investigation. Essentially, the image processing exercise involved application of a user-defined routine in a commercial software platform which included operations of image enhancement, filtering, thresholding and object identification. In the processed images, each of the dimples could be delineated and their dimensions measured (Fig. 4a3 and b3). The measurements obtained were statistically analysed to provide the distribution of dimple sizes. The ductile tearing ridge features (i.e., the two dimensional boundary of different sized dimples spread throughout the fracture surfaces) appear brighter in the relatively grey background of the dimples (Fig. 4). Many

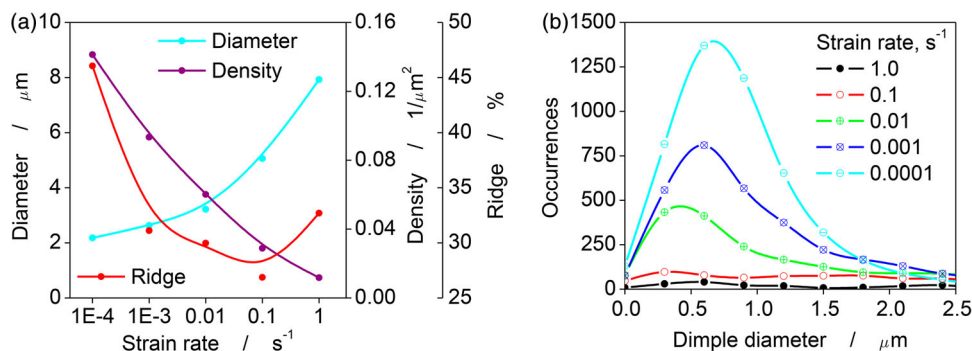
representative fractographs were captured at different strain rate conditions under SEM from the centre of the fractured specimens. These fractographs were analysed off-line after appropriate grey thresholding to obtain the reasonable area fraction of the extent of ductile tearing ridges. The grey thresholding was done properly in such a manner so that all the dimple boundaries were filled in properly. The linear intercept method (i.e., point counting) was also employed to reproduce the results obtained through image analysis to measure the ductile tearing ridge content.

## Results and discussion

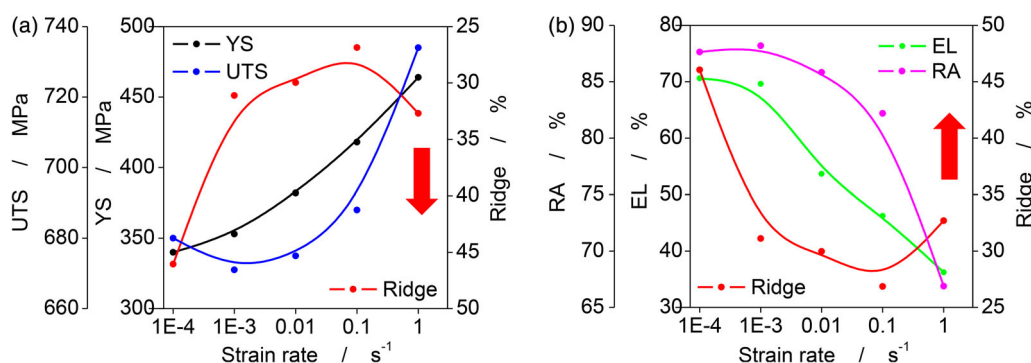
Fractographs at selected strain rate conditions (i.e., 0.0001 and 1.0 s<sup>-1</sup>) and their corresponding dimple network, fracture ridge morphologies/pattern as processed through image processing, is shown in Fig. 4. It is observed from Fig. 5 that the mean dimple diameter increases with the strain rate, the minimum being at the lowest strain rate. It has also been observed that with the increase in strain rate, the extent of tearing ridge is decreasing (Fig. 5) (also visual impression from Fig. 4). These show the fracture surfaces of materials failing by ductile manner is covered by segments of different sized dimples which coalesced to produce the fracture path/ridge. It has been observed from all the fracture surfaces that the shape of the dimples is primarily spherical and of non-uniform size (i.e., irregular topography depending upon the strain rate imposed and the inhomogeneous



4 Representative SEM fractographs (secondary image) of the specimen tested at strain rate of: a1 0.0001 s<sup>-1</sup> and b1 1.0 s<sup>-1</sup>, a2 and b2 corresponding fracture ridges (black), respectively and a3 and b3 corresponding dimple networks, respectively. Image processed fractographs: a2, b2, a3 and b3



5 a Relation between dimple density, dimple diameter and the extent of fracture ridge with strain rates. b Dimple size distribution at various strain rates<sup>1</sup>



6 a Variation of strength and b ductility properties with the extent of fracture ridges at various strain rates. YS: yield strength; UTS: ultimate tensile strength; EL: elongation and RA: reduction in area

distribution of DIM plates). The large and elongated dimples displayed on the fractographs differ markedly from the small and more circular dimples observed on the fracture surface in two dimensions. According to Benson,<sup>25</sup> the fracture surface, which is created by void linking through growth or material failure, is a strong function of the magnitude of the stress wave. The directional character of dimples on the rupture surface strongly depends on the loading character (*i.e.*, strain rates) which caused the plastic flow and the inhomogeneous spatial distribution of DIM in the austenite matrix. The shape of the dimples depends upon the state of stress-state of strain conditions. According to Garrison and Wojcieszynski,<sup>17</sup> the characteristics of inclusions which influence the fracture toughness of a material are volume fraction, their spacing and the resistance to void nucleation. Lee *et al.*<sup>26</sup> have noticed a decrease in the depth and density of dimples on the fracture surface of austenitic stainless steel with increasing strain rate and a corresponding strain rate dependency of the mechanical properties. Micro void nucleation and growth are dictated by the plastic strain and the hydrostatic tensile stress. According to Rice and Tracy,<sup>27</sup> void growth increases with increasing particle size. The evolution of local plastic strain and hydrostatic stress, in turn, is controlled by the dislocation population and their interactions. Since the same phenomena (*i.e.*, dislocation population and their interactions) are also responsible for the mechanical properties of the material, it is anticipated that a correlation exists between the mechanical properties and the fracture features on the ductile fracture surface.<sup>19</sup> Anderson<sup>7</sup> concluded that the process of ductile fracture constituting

the stages of void nucleation and growth are predominantly influenced by the nature of dislocation–particle and dislocation–dislocation interactions, which in turn are governed by the state of strain hardening in a material. Spitzig *et al.*<sup>28</sup> examined the effect of sulphur content and inclusion volume fraction on the charpy impact energy of AISI 4340 steel. Argon *et al.*<sup>29</sup> have addressed many of the specific micro-mechanical aspects of creep cavity nucleation.

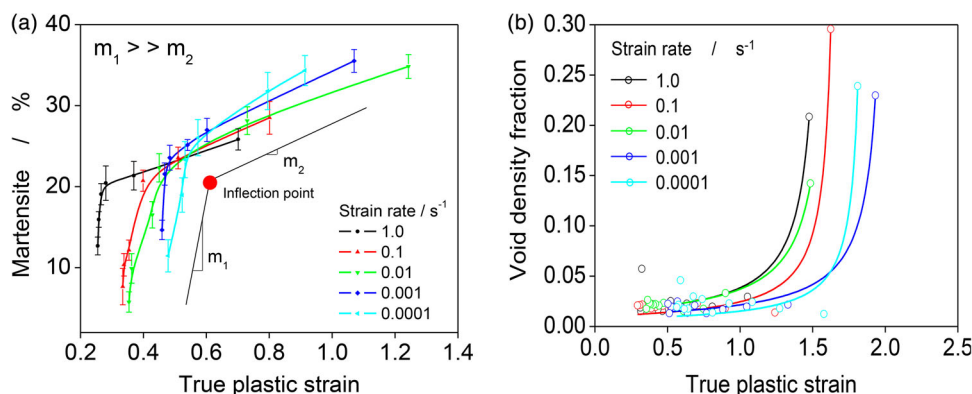
Figure 6a shows the variation of strength properties (YS and UTS) with the extent of fracture ridge (note the right Y-axis); Fig. 6b shows the corresponding variation in ductility properties (EL and RA). It should be noted that the amount of fracture ridge decreases with increasing strain rate (Figs. 4 and 5a). This nature of variation of fracture ridge with strain rate is precisely inverse to that of the strength properties and similar to that of the ductility properties. The clear correlation between the extent of fracture ridge, dimple size and density as a function of strain rate is represented in Fig. 5a. With increasing strain rate, since the dimple density is decreased, the interligament available between dimples is expected to be more. The propensity of voids for equatorial growth thereby increases at higher strain rates. The smaller dimples link rapidly and, hence lead to lower ductility. It has been found that dimple density and the extent of fracture ridge variation is similar kind with the strain rate. It is indeed observed from Fig. 5a that with increase in strain rate, the mean dimple size increases with simultaneous lowering of dimple density. The dimple diameter distributions for tests at various strain rates are shown in Fig. 5b. It has been found that the mean dimple diameter

increases with the strain rate, the minimum being at the lowest strain rate ( $0.0001 \text{ s}^{-1}$ ). The pattern and size distribution of the dimples on the fracture surfaces resulting variation in roughness at various strain rates reflect the distribution of DIM plates on the austenite matrix. E-Soudani and Pelloux<sup>30</sup> have derived a complex relationship between the fracture surface roughness and the linear roughness in their elegant study. Figure 2c as evidence clearly shows the nucleation of voids from the martensite plates, which is encircled and marked. According to Jamal *et al.*<sup>31</sup> the number density of pull-outs of martensite/ferrite colonies observed in the tensile fracture surfaces quantitatively correlates with the variability in the tensile ductility, and therefore, it accounts for a significant part of the observed variability in the ductility of DP980 steels.

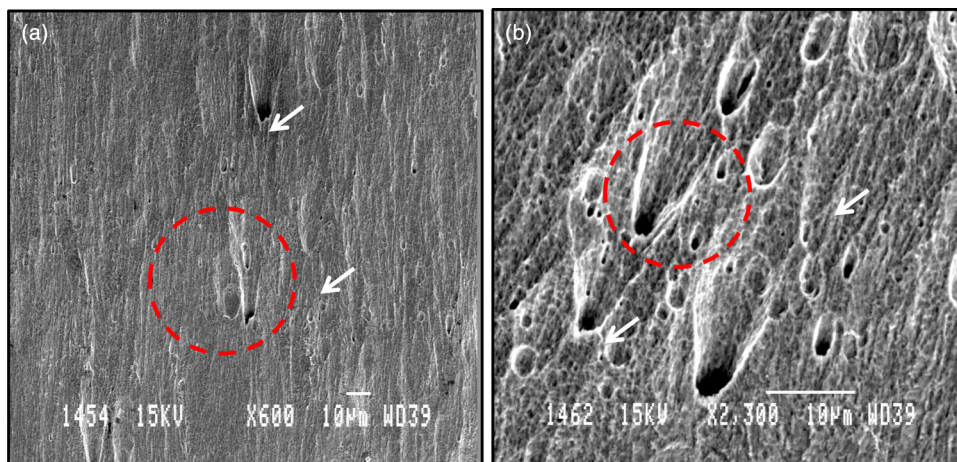
This kind of behaviour is attributed to the DIM transformation of the present metastable alloy. The non-uniform distribution of DIM plates (Fig. 3) indicates the inhomogeneous nature of deformation in micro-scale and crystallographic *variant selection*, which has been extensively discussed by the present alloy elsewhere.<sup>32,33</sup> The *variant selection* of martensite is schematically shown in Fig. 1. When the material is prone to stress-induced phase transformation, most of the tiny voids which are formed while uniaxial loading at the martensite nucleation sites (Fig. 2c) do not always link rapidly because the high amount of martensite formed at the irregular void periphery (i.e., due to high plastic strain) promote growth of voids that lead to higher ductility. Lindley *et al.*<sup>34</sup> demonstrated that it is the interaction between the particles and matrix deformation which leads to void nucleation. Birkle *et al.*<sup>35</sup> identified the characteristics distance as the inclusion spacing and discussed their fracture toughness dependency with this as a function of tempering temperature.

Figure 7a represents the effect of strain rate on DIM formation as a function of true strain. Irrespective of strain rate, the nature of variation of DIM with true plastic strain is almost identical. At lower strain levels, the amount of DIM increases rapidly in a linearly proportional manner, after which the rate of transformation decreases. It is well established that at the initial stage of deformation,  $\epsilon$  (hcp) martensite is formed and as the deformation progress,  $\alpha'$  (bcc) martensite is formed. On comparing all the curves (Fig. 7a), it has been observed that while the increase in strain rate favours DIM

nucleation at lower strain, the maximum amount of DIM formed under tension is reduced with increasing strain rate.<sup>1-3</sup> This is mainly attributed to the local variation of stacking fault energy (SFE) of the material, which has been modelled and critically reviewed by the present author elsewhere.<sup>36</sup> At higher strain rate, the heat of deformation is retained in the specimen and temperature increases during plastic deformation. Austenite stability increases because of this, and less martensite is formed. The inflections shown in the curves (Fig. 7a), indicating sluggish transformation after a critical level of plastic deformation which depends upon the strain rate, and the reduced amount of martensite formation with increasing strain rate are attributed to this local rise in temperature (i.e., adiabatic heat). Guntur and Reed<sup>37</sup> proposed that the initial easy deformation stage is due to the  $\epsilon$  (hcp) martensite formation and the rapid hardening stage is due to the evolution of  $\alpha'$  (bcc) martensite formation, since  $\epsilon$  (hcp) martensite tends to disappear at the beginning of the rapid hardening stage. The measured evolution of the density fraction of voids nucleated by the interface decohesion at DIM plates is represented by the data points in Fig. 7b for all the strain rates. Micro void formation associated with martensite resulted from either decohesion at the austenite–martensite interface or from the separation of adjacent islands and localised deformation of martensite is shown in Figs. 2c and 8. Garrison *et al.*<sup>38</sup> showed that the number and area fractions of damage particles increase significantly with the decrease in temperature for cast A356 aluminium alloy. Just near the fracture surface, the sample was polished and etched and it shows the void nucleating sites from martensite plates. The rate of development of the void population with true plastic strain is initially low, and then increases rapidly with the high strains on approaching the fracture surfaces. For the same amount of true strain, void density fraction was found to be maximum for the high strain rate specimen compared to low strain rate. It is also noted that to reach the same amount of void density fraction, higher strain rate specimen needs less amount of true plastic strain accumulation than lower strain rates. The details have been discussed elsewhere.<sup>3</sup> Spitzig *et al.*<sup>28</sup> have shown that the void growth rate increases with increasing initial porosity for porous iron. Void growth rate increases with increasing initial void size.<sup>39,40</sup> Therefore, an increase of the void growth rate



7 a Extent of DIM as a function of true plastic strain for all strain rates.<sup>1</sup> Extensive image processing has been employed to measure DIM and b void density fraction as a function of true plastic strain for all strain rates.<sup>3</sup> Archimedes's principle has been used to measure the void density



8 Void nucleating sites (DIM plates) near the fracture surface; voids (red encircled) and DIM (arrow). a Lower magnification and b higher magnification

with increasing martensite lath size should be expected. According to Liu *et al.*,<sup>41</sup> the influence of void size depends strongly on the stress triaxiality ratio. Large increases in ductility (Fig. 6b) are achieved when the cavity nucleation is delayed/suppressed (Fig. 7b). As the volume fraction of DIM increases (Fig. 7a), the nucleation rate decreases. Cox and Low<sup>40</sup> experimentally determined void nucleation data as a function of strain for a commercial grade and high purity grade of AISI 4340 steel. According to Avramovic-Cingaraa *et al.*,<sup>42</sup> the steel with more uniform distribution of martensite plates showed a slower rate of damage growth and a continuous void nucleation during the deformation process, which resulted in a higher void density before fracture. As seen by Avramovic-Cingara *et al.*,<sup>42</sup> void nucleation in dual phase steels occurred during the entire deformation process. According to Edelson and Baldwin,<sup>43</sup> the total strain to fracture in a particular metal depends primarily on the proportion of second-phase particles or inclusions in the ductile matrix; the greater the concentration of particles, the lower the strain to fracture. By systematically varying the martensite volume fraction, Erdogan and Tekeli<sup>44</sup> showed that an enhanced strength and ductility can be achieved when more martensite is present. Similar observations where martensite promotes void nucleation are also reported by Poruks *et al.*<sup>45</sup> in low carbon bainitic steel.

## Conclusions

The experimental research on the relative contribution of DIM to the fracture appearance of metastable austenitic stainless steels at different strain rates under tension is presented. Based on these, the following concluding remarks can be made:

- (i) The extent of *ductile tearing ridges* morphologies on the fracture surfaces reflects the multiplicity of DIM nucleation, which contributes significantly to the deformation and fracture behaviour of the material.
- (ii) Different dimple sizes are observed on the fracture surfaces at various strain rates due to the variation in DIM content as void nucleating sites.

- (iii) A systematic correlation exists for the void density fraction and the DIM volume fraction as functions of strain and strain rate.
- (iv) An appropriate fractographic investigation can be employed to make a reasonable estimate of the mechanical properties of a material.

## Acknowledgements

All the experiments were carried out at CSIR-National Metallurgical Laboratory, Jamshedpur when the author was previously employed (2004–2014). The author expresses his gratitude to Dr S. Tarafder, Chief Scientist and Dr S. Sivaprasad, Senior Principal Scientist of CSIR-NML for fruitful suggestions/discussions during experimentations. The author would also like to thank all the respected reviewers for their strong recommendations which helped a lot to prepare the revised manuscript.

## References

1. A. Das and S. Tarafder: 'Experimental investigation on martensitic transformation and fracture morphologies of austenitic stainless steel', *Int. J. Plast.*, **2009**, **25**, 2222–2247.
2. A. Das and S. Tarafder: 'Geometry of dimples and its correlation with mechanical properties in austenitic stainless steel', *Scr. Mater.*, **2008**, **59**, 1014–1017.
3. A. Das: 'Martensite–void interaction', *Scr. Mater.*, **2013**, **68**, 514–517.
4. A. L. Gurson: 'Continuum theory of ductile fracture by void nucleation and growth', *Trans. ASME, J. Eng. Mater. Technol.*, **1977**, **99**, 2–15.
5. W. M. Garrison Jr. and N. R. Moody: 'Ductile fracture', *J. Phys. Chem. Solids*, **1987**, **48**, 1035–1074.
6. S. H. Goods and L. M. Brown: 'The nucleation of cavities by plastic deformation', *Acta Mater.*, **1979**, **27**, 1–15.
7. T. L. Anderson: 'Fracture mechanics: fundamentals and applications', 3rd edn, 265; **1995**, Boca Raton, NY, CRC Press.
8. W. M. Garrison Jr. and A. L. Wojcieszynski: 'A discussion of the effect of inclusion volume fraction on the toughness of steel', *Mater. Sci. Eng. A*, **2007**, **464**, 321–329.
9. A. Das, S. Sivaprasad, M. Tarafder, S. K. Das and S. Tarafder: 'Estimation of damage in high strength steels', *Appl. Soft. Comput.*, **2013**, **13**, 1033–1041.
10. A. Das, S. K. Das, S. Sivaprasad, M. Tarafder and S. Tarafder: 'Analysis of damage accumulations in high strength low alloy steels under monotonic deformation', *Proc. Eng.*, **2013**, **55**, 786–792.

11. A. Das, T. Chowdhury and S. Tarafder: 'Ductile fracture micro-mechanisms of high strength low alloy steels', *Mater. Des.*, **2014**, **54**, 1002–1009.
12. A. Das, S. K. Das, S. Sivaprasad and S. Tarafder: 'Fracture-property correlation in copper strengthened high-strength low-alloy steel', *Scr. Mater.*, **2008**, **59**, 681–683.
13. A. Das, S. K. Das and S. Tarafder: 'Correlation of fractographic features with mechanical properties in systematically varied microstructures of Cu-strengthened high-strength low-alloy steel', *Met. Mater. Trans. A*, **2009**, **40**, 3138–3146.
14. A. Das, S. Sivaprasad, P. C. Chakraborti and S. Tarafder: 'Correspondence of fracture surface features with mechanical properties in 304LN stainless steel', *Mater. Sci. Eng. A*, **2008**, **496**, 98–105.
15. J. L. Maloney and W. M. Garrison, Jr.: 'The effect of sulphide type on the fracture behaviour of HY 180 steel', *Acta Mater.*, **2005**, **53**, 533–551.
16. N. R. Moody, W. M. Garrison Jr., J. E. Costa and J. E. Smugeresky: 'The role of defect size on the fracture toughness of powder processed Ti-10V-2Fe-3Al', *Scr. Mater.*, **1989**, **23**, 1147–1150.
17. W. M. Garrison Jr. and A. L. Wojcieszynski: 'A discussion of the spacing of inclusions in the volume and of the spacing of inclusion nucleated voids on fracture surfaces of steels', *Mater. Sci. Eng. A*, **2009**, **505**, 52–61.
18. A. Das and P. Poddar: 'Structure–wear–property correlation', *Mater. Des.*, **2013**, **47**, 557–565.
19. A. H. Cottrell: 'Theoretical aspects of fracture', in 'Fracture' (ed. B. L. Averbach, D. R. Felbeck, G. T. Hahn and D. A. Thomas), **20: 1959**, New York, The Technological Press of MIT and John Wiley and Sons, Inc.
20. A. A. Benzerga, J. Besson and A. Pineau: 'Anisotropic ductile fracture. Part I: experiments', *Acta Mater.*, **2004**, **52**, 4623–4638.
21. A. Das, N. Roy and A. K. Ray: 'Stress induced creep cavity', *Mater. Sci. Eng. A*, **2014**, **598**, 28–33.
22. D. Lassance, D. Fabregue, F. Delannay and T. Pardoën: 'Micromechanics of room and high temperature fracture in 6xxx Al alloys', *Prog. Mater. Sci.*, **2007**, **52**, 62–129.
23. D. A. Curry, I. Milne and R. S. Gates: 'The influence of a high loading rate on the fracture behaviour of a pressure vessel steel', *Mater. Sci. Eng.*, **1984**, **63**, 101–109.
24. G. E. Dieter: '*Mechanical metallurgy*', SI Metric Edition, 145; **1993**, Berlin, Springer.
25. D. J. Benson: 'An analysis of void distribution effects on the dynamic growth and coalescence of voids in ductile metals', *J. Mech. Phys. Solids*, **1993**, **41**, 1285–1308.
26. W.-S. Lee, C.-F. Lin and T. J. Liu: 'Strain rate dependence of impact properties of sintered 316L stainless steels', *J. Nucl. Mater.*, **2006**, **359**, 247–257.
27. J. R. Rice and D. M. Tracy: 'On the ductile enlargement of voids in triaxial stress fields', *J. Mech. Phys. Solids*, **1969**, **17**, 201–217.
28. W. A. Spitzig, R. E. Smelser and O. Richmond: 'The evolution of damage and fracture in iron compacts with various initial porosities', *Acta Mater.*, **1988**, **36**, 1201–1211.
29. A. S. Argon, J. Im and R. Safoglu: 'Cavity formation from inclusions in ductile fracture', *Mater. Trans. A*, **1975**, **6**, 825–837.
30. S. M. El-Soudani and R. M. Pelloux: 'Influence of inclusion content on fatigue crack propagation in aluminium alloys', *Metall. Trans.*, **1973**, **4**, 519–531.
31. R. S. Jamwal, A. M. Gokhale and S. P. Bhat: 'Quantitative fractographic analysis of variability in the tensile ductility of a high strength dual phase steel', *Metallogr. Microstr. Anal.*, **2013**, **2**, 30–34.
32. A. Das: 'Crystallographic variant selection of martensite during fatigue deformation', *Philos. Mag.*, **2015**, **95**, 844–860.
33. A. Das: 'Crystallographic variant selection of martensite at high stress/strain', *Philos. Mag.*, **2015**, **95**, 2210–2227.
34. T. C. Lindley, T. Oates and C. E. Richards: 'A critical appraisal of carbide cracking mechanisms in ferride/carbide aggregates', *Acta Met.*, **1970**, **18**, 1127–1136.
35. A. J. Birkle, R. P. Wei, G. E. Pellissier: 'Analysis of plane strain fracture in Ni–Cr–Mo alloys', *Trans. ASM*, **1966**, **59**, 981–990.
36. A. Das: 'Revisiting stacking fault energy of steels', *Met. Mater. Trans. A*, **2016**, **47**, 748–768.
37. C. J. Guntur and R. P. Reed: 'The effect of experimental variables including the martensitic transformation on the low-temperature mechanical stainless steel', *Trans. ASM*, **1962**, **55**, 399–419.
38. A. M. Garrison, M. D. Manish and M. F. Horstemeyer: 'Effect of temperature on silicon particle damage in A356 alloy', *Met. Mater. Trans. A*, **1998**, **29**, 905–907.
39. T. B. Cox and J. R. Low: 'An investigation of the plastic fracture of AISI 4340 and 18 Nickel-200 grade maraging steels', *Metall. Trans.*, **1974**, **5**, 1457–1470.
40. R. H. Vanstone, T. B. Cox, J. R. Low and J. A. Psioda: 'Microstructural aspects of fracture by dimpled rupture', *Int. Met. Rev.*, **1985**, **30**, 157–179.
41. B. Liu, Y. Huang, M. Li, K. C. Hwang and C. Liu: 'A study of the void size effect based on the Taylor dislocation model', *Int. J. Plast.*, **2005**, **21**, 2107–2122.
42. G. Avramovic-Cingara, C. A. R. Saleh, M. K. Jain and D. S. Wilkinson: 'Void nucleation and growth in dual-phase steel 600 in uniaxial tension', *Met. Mater. Trans. A*, **2009**, **40**, 3117–3127.
43. B. Edelson and W. M. Baldwin: 'The effect of second phases on the mechanical properties of alloys', *Trans. Am. Soc. Metal.*, **1962**, **55**, 230–250.
44. M. Erdogan and S. Tekeli: 'The effect of martensite particle size on tensile fracture of surface-carburised AISI 8620 steel with dual phase core microstructure', *Mater. Des.*, **2002**, **23**, 597–604.
45. P. Poruks, I. Yakubtsov and J. D. Boyd: 'Martensite–ferrite interface strength in a low carbon bainitic steel', *Scr. Mater.*, **2006**, **54**, 41–45.